Anal Bioanal Chem (2016) 408:2195–2201
DOI 10.1007/s00216-016-9366-6

RAPID COMMUNICATION

In situ monitoring, separation, and characterization of gold nanorod transformation during seed-mediated synthesis

Thao M. Nguyen[1,2] · **John M. Pettibone**[1] · **Julien Gigault**[3] · **Vincent A. Hackley**[1]

Received: 25 September 2015 / Revised: 21 January 2016 / Accepted: 26 January 2016 / Published online: 12 February 2016

Abstract The control of gold nanorod (GNR) solution-based syntheses has been hindered in part by the inability to examine and control the conversion of precursor seed populations to anisotropic materials, which have resulted in low yields of desired products and limited their commercial viability. The advantages offered by tandem separation and characterization methods utilizing asymmetric-flow field flow fractionation (A4F) are principally achieved as a result of their non-disruptive nature (minimizing artefacts), fast throughput, and in-situ analysis. With hyphenated A4F methods, resolved populations of seeds and secondary products, up to long aspect ratio rods, have been achieved and exemplify progress towards elucidating mechanistic aspects of formation and thus rational design. While there have been previously reported studies on A4F separation of GNRs, to our knowledge, this is the first published investigation of in situ GNR growth, separation, and characterization based on A4F, where its utilization in this capacity goes beyond traditional separation analysis. By using hydroquinone as the reducing agent, the conversion of the initial seed population to a distribution of products, including the GNRs, could be monitored in real time using A4F hyphenated with a diode array detector. Transmission electron microscopy confirms that the number of peaks observed during fractionation corresponds with size and shape dispersity. This proof-of-principle study introduces A4F as a technique that establishes a foundation for future mechanistic studies on the growth of GNRs from gold seeds, including conversion of the seed population to initial products, a topic highly relevant to advancing progress in nanomanufacturing.

Keywords Field flow fractionation · Gold nanorod · Nanomanufacturing · Nanomaterial · Seed-mediated growth · Separation · Transformation

Introduction

A fundamental goal of nanotechnology is rational control over the size and shape of nanoscale particles (NPs); this requires a comprehensive understanding of underlying growth mechanisms [1–4]. Gold nanorods (GNRs) represent a commercially important subset of nanomaterials that possess tunable properties for broad applications in sensing, biomedical imaging, drug delivery and photothermal therapy [5–12]. Photochemical, electrodeposition, and seed-mediated synthetic routes have been reported, along with evolving methodology that is largely empirically driven, but the detailed mechanistic understanding required to attain rational control of GNR shape and product distribution remains surprisingly elusive [13]. While a body of work exists regarding the mechanisms and growth kinetics of gold NPs, the reports on GNR transformations are sparse [3, 14, 15]. Here, we demonstrate that hyphenated asymmetric-flow field flow fractionation

Electronic supplementary material The online version of this article (doi:10.1007/s00216-016-9366-6) contains supplementary material, which is available to authorized users.

✉ Vincent A. Hackley
vince.hackley@nist.gov

[1] Materials Measurement Science Division, National Institute of Standards and Technology, 100 Bureau Drive, Gaithersburg, MD 20899-8520, USA

[2] Present address: ANSER, 5727 Leesburg Pike N-5000, Falls Church, VA 22041, USA

[3] Laboratoire de Physico- et Toxico-Chimie de l'Environnement, Université de Bordeaux, CNRS, 351 Cours de la Libe'ration, Talence 33405, France

(A4F), a hydrodynamic separation technique, has the capacity to probe the in situ transformation of distinct populations of precursor seeds and intermediate products to GNRs, providing essential information for their further application and the development of sustainable nanomanufacturing.

The seed-mediated approach is commonly utilized, but is possibly the most difficult to reproduce due to the large number of kinetic and thermodynamic factors that contribute to creating uniform initial seed populations and their subsequent growth to narrow product distributions, which include anisotropic species. It is well established that the nature and size of gold seeds strongly affect the yield, aspect ratio, and defect structures of resulting products, [16, 17] which yield a distribution of product shapes, such as rods, spheres, prisms, and plates. Thus, significant effort has been expended to control secondary processing procedures (post-nucleation) including thermal, [18] laser heating (photothermal), [19] cyanide, [20] persulfate and oxygen, [21] oxidative dissolution using H_2O_2, [22] and ligand exchange [23]. The conversion of GNRs via these processes is typically monitored using UV-Vis absorbance, dynamic light scattering, scanning electron microscopy and transmission electron microscopy (TEM), but inherent difficulties exist. For EM measurements, continual growth or processing during sample preparation can occur [2] and significant efforts are required for obtaining statistically meaningful results across the polydisperse product distributions produced in GNR syntheses. Some success has been realized with cryo-TEM, [24] but in practice this is not amendable to analyzing large numbers of NPs, let alone the bulk sample in its entirety. Because parameter control is difficult, even borderline intractable to date, research efforts have been focused on post-synthesis separation processes, such as analytical centrifugation and density gradients [25–27].

Hyphenated A4F methods have the ability to overcome two limitations and constraints inherent in EM: sample perturbation and the challenge of accurately assessing the entire sample, from seeds to high aspect ratio (AR) structures. However, microscopy is still useful to visually validate the separation procedures of different shapes in the complex reaction mixture. Previously published studies have established the potential for application of A4F to the separation and characterization of GNRs [28–31]. Runyon et al., [28] examined the relationship between retention time and the effective hydrodynamic size of seed-grown GNRs. They also compared theoretical predictions of surface plasmon resonance (SPR) absorbance against measurements of fractionated GNRs characterized by a narrow AR. However, this study did not address the seed-mediated growth process, but rather focused on fractionating the end product of the reaction. Here we use Au^{3+} reduction by hydroquinone [23] (Hq) to monitor the temporal evolution of high aspect ratio (AR > 5) GNR production, which has shown promise for creating higher AR species than ascorbic acid initiated growth, and occurs on a time scale more compatible for A4F evaluation. To our knowledge this is the first reported study to apply A4F to directly probe seed-mediated growth of GNRs, and is proof-of-principle for more detailed studies of the kinetics and growth mechanisms associated with these commercially important reactions.

Materials and methods

Ammonium nitrate (NH_4NO_3, 99 %), hydroquinone (Hq) (99 %), sodium hydroxide (NaOH), hydrogen chloride (HCl), sodium borohydride ($NaBH_4$), and 0.2-μm regenerated cellulose filters were purchased from VWR (Bridgeport, NJ).[1] Cetyl trimethyl ammonium bromide (CTAB) was purchased from Acros Organics (Geel, Belgium). Hydrogen tetrachloroaurate trihydrate ($H[AuCl_4]\cdot 3H_2O$, 99.99 %) and silver nitrate ($AgNO_3$, 99 %) were purchased from Sigma-Aldrich (St. Louis, MO). Deionized water used in all experiments was generated by a biological grade water purification system with ultra-low total organic carbon from Aqua Solutions (Jasper, GA). All chemicals were used without further purification, and other then gold and CTAB, all solutions were prepared fresh daily. Commercially synthesized CTAB stabilized GNRs were purchased from Nanopartz (Loveland, CO).

Fractionation was performed with an Eclipse 3+ (Wyatt Technology, Santa Barbara, CA) A4F system, equipped with an Agilent Technologies Inc. (Santa Clara, CA) 1100 series isocratic pump and Gastorr degasser (TG-14, Flom Co., Ltd., Tokyo, Japan). A Rheodyne 7725i manual injection valve with a 100 μL stainless steel sample loop (IDEX Corporation, Oak Harbor, WA) was used for sample introduction. Polyethersulfone (PES) membranes were purchased from Wyatt Technology. Eluted samples were monitored with an Agilent 1200 series UV–Vis absorbance diode array detector (DAD), with a spectral range from 190 to 950 nm and a sampling rate of 20 Hz. TEM images were collected using a JEM 3010 from JEOL (Waterford, VA) operated at 300 kV.

Synthesis of GNRs

The seed-mediated growth procedure was adapted from Vigderman et al. [23] Briefly, a solution of 0.01 mol L^{-1} $NaBH_4$ in 0.01 mol L^{-1} NaOH was freshly prepared. To 5 mL of 50 mmol L^{-1} $HAuCl_4$ in 0.1 mol L^{-1} CTAB under rapid stirring at 1000 rpm (104.7 rad s^{-1}) was added 500 μL of the $NaBH_4$ solution, leading to a color change from dark yellow to light brown. The product of this reaction is the seed solution. To synthesize the GNRs, 70 μL of 0.1 mol L^{-1} $AgNO_3$ was added to 10 mL of 0.5 mmol L^{-1} $HAuCl_4$ in

[1] The identification of any commercial product or trade name does not imply endorsement or recommendation by the National Institute of Standards and Technology.

0.1 mol L^{-1} CTAB. To this solution, 500 μL of 0.1 mol L^{-1} Hq was added and the solution was gently stirred until it became clear, indicating the reduction of Au^{3+} to Au^{+} and yielding the growth solution. Finally, to initiate growth of GNRs, 160 μL of the seed solution was added to the growth solution, mixed thoroughly, and allowed to react for up to 72 h.

Characterization

Samples for analysis were prepared by withdrawing 1 mL from the reaction vial following addition of the seeds to the growth solution at 30 min, 1 h, 2 h, 20 h, and 72 h. The aliquots were centrifuged immediately at 6000 rpm (628.2 rad s^{-1}) for 5 min. The supernatant was discarded to remove Hq and quench the reduction reaction. The supernatant was replaced by 0.15 mmol L^{-1} of CTAB and centrifuged again for 5 min. The resulting pellet was dispersed in 1 mmol L^{-1} CTAB and used in the fractionation studies and for TEM analysis. Samples were prepared for TEM by pipetting 6 μL of the GNR suspension onto a lacey carbon coated copper grid (Electron Microscopy Sciences, Hatfield, PA) and air dried at room temperature.

Fractionation

The retention of the reaction products was evaluated in a mobile phase consisting of 0.15 mmol L^{-1} CTAB and 0.35 mmol L^{-1} NH_4NO_3 prepared with ultrapure DI water (18 MΩ.cm); the mobile phase solution was initially passed through a 0.2 μm regenerated cellulose filter. This mobile phase composition was previously determined to be optimal for the separation of CTAB coated GNRs [29]. Previous experiments indicated that an ionic strength of 0.5 mmol L^{-1} provided optimal resolution and recovery. Further studies demonstrated that CTAB in combination with an inert salt (NH_4NO_3) provide optimal control of GNR/CTAB-membrane interactions. The mobile phase composition selected for this study aims to strike a balance between overly repulsive interactions that result in poor retention and attractive interactions that result in poor recovery. After preliminary testing, a 250 μm thick spacer was selected, where channel dimensions are 26 cm in length and from 2 cm to 1 cm in width. This spacer provides efficient fractionation with less dilution of the analyte, resulting in better sensitivity, compared with the 350 μm spacer typically used for fractionation of nanoscale particles. The improved sensitivity must be balanced against the reduced resolution. PES membranes with a 10 kDa cut-off were used for all experiments. Optimized A4F fractionation parameters and conditions are presented in Table S1 of the Electronic Supplemental Material (ESM): Fig. S1 in the ESM includes details for the fractionation of the seed population using a 490 μm spacer. An initial elution step prior to focusing is used to ensure that any residual sample from previous runs is washed out prior to the next analysis. The focusing period that comprises a 0.2 min mL^{-1} injection of 100 uL of sample under focusing at 2 mL min^{-1} proceeded by an additional 5 min of focus was used to ensure sample components achieved equilibrium states between the diffusive forces acting away from the membrane wall and the hydrodynamic forces acting towards the wall. After focusing, separation mode was initiated by applying the fixed 0.5 mL min^{-1} main carrier flow velocity (V_p) (laminar) and cross flow (V_c) in the channel, which were optimized following our previously published protocol [32].

Results and discussion

GNR growth with addition of Hq occurs over a time scale of days and can be visualized by representative TEM images (Fig. 1). In Fig. 1a, the gold species remain small (less than 5 nm) and undeveloped at 30 min. By $t = 2$ h, where $t = 0$ is time of Hq addition, the seeds have grown into clearly faceted objects and the characteristic NR morphology has become evident. UV-Vis spectra also contain absorbance peaks near 600 nm that are characteristic of the triangular nanoplate SPR signatures with edges ranging from 40 to 120 nm [33, 34]. By $t = 6$ h, the average size of the NPs and rods have increased to ≈ 50 nm in length and diameter. Finally, the final unpurified product at 72 h displays an array of shapes having variable sizes (Fig. 1d and S2). This is a typical yield for seed-mediated products reported in the literature, and demonstrates the necessity for post-synthesis processing or purification to enrich the desired species.

The advantage of using A4F for GNR formation is the capacity for simultaneous in situ separation and characterization. Monitoring of absorbance signatures online provides a quick assessment tool to examine the quality (i.e., relative abundance of analytes) and heterogeneity of the sample. Figure 2 illustrates a comparison of online 3D UV-Vis absorbance spectra for GNR synthesis from the same production batch at $t = 2$ h and 72 h. While absorbance at 520 nm is used primarily to monitor spherical gold NPs and the transverse surface plasmon resonance (TSPR) band of the resulting GNRs, the longitudinal SPR (LSPR) of GNRs, which spans from 600 nm into the near-IR range, can be used to monitor the growth of GNRs. At the optimized fractionation condition, the formation of GNRs is clearly visible over the entire DAD range. At $t = 2$ h, the DAD response between 400 and 520 nm remains jagged and unresolved, supported by the similar sizes of the nanostructures as confirmed in Fig. 1b. Under the same fractionation condition at $t = 72$ h, the UV-Vis spectra reveal resolved peaks and separation with an absorbance signature up to 800 nm. In following the evolution of fractionation peaks with time, these results suggest the first discriminative

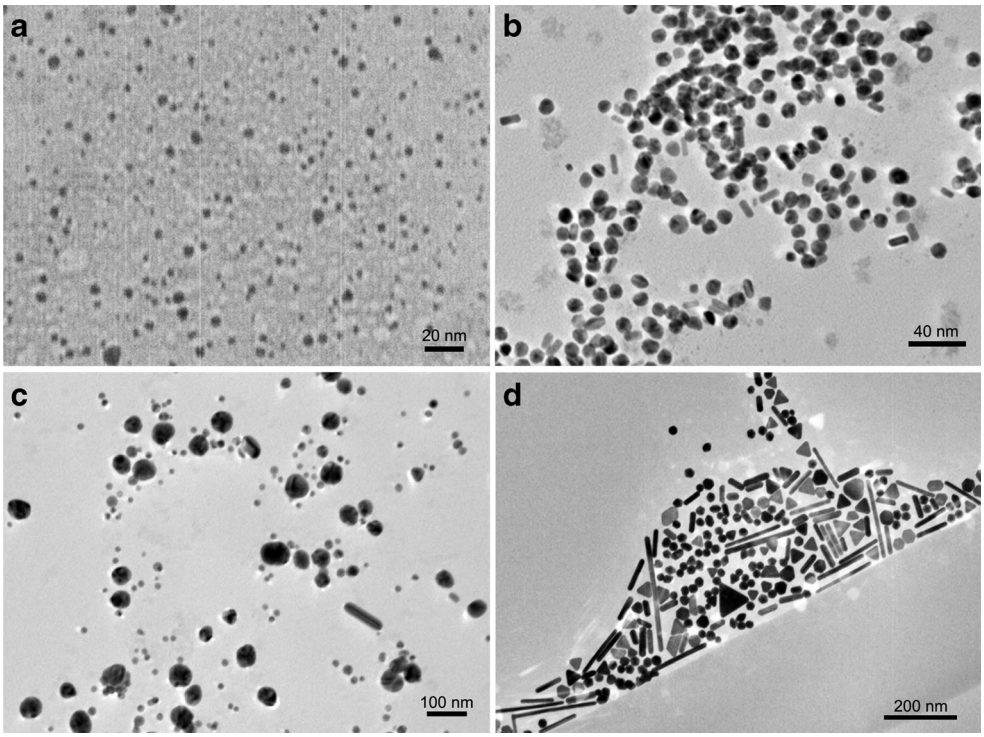

Fig. 1 Representative TEM images of GNR samples taken at **a** 30 min, **b** 2 h, **c** 6 h, and **d** 72 h after the addition of Hq to the seeds. Scale bars: **a** 20 nm, **b**, 40 nm, **c** 100 nm, and **d** 200 nm

separation and in situ monitoring of the transformation from seeds to GNRs, which should lead to a better understanding of the evolving structure-property relationships of distinct populations that yield disparate product distributions from seemingly uniform seeds.

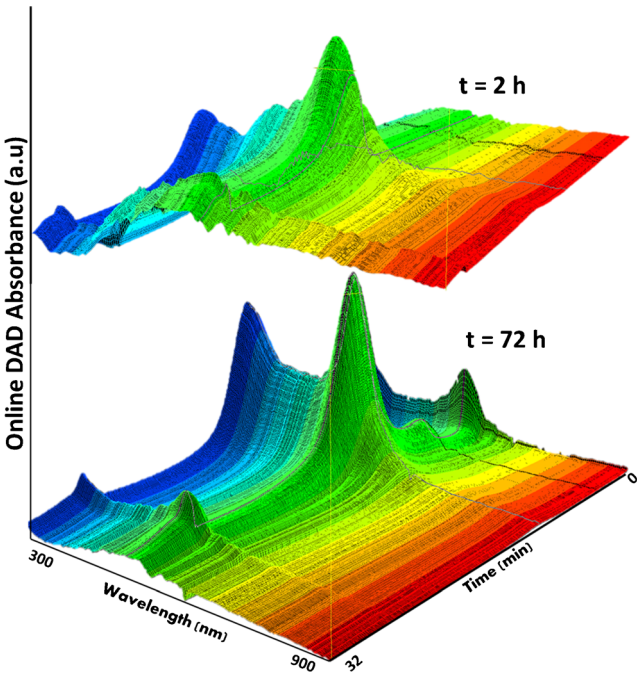

Fig. 2 3D UV-Vis absorbance spectra of synthesis solution 2 h and 72 h after the addition of Hq. The broad peaks and similar elution time of the species indicate that at 2 h the products are of similar size. The multiple peaks from 400 nm through 700 nm demonstrate the ability of A4F in detecting the presence and formation of varying populations of gold nanostructures. At 72 h, clearly resolved populations become evident

Figure 3a illustrates the first two time points examined. Since the TSPR band for GNRs overlaps with the characteristic SPR band for spheroidal NPs, a LSPR band in the near-IR range (800 nm) was used as a trace for the formation of GNRs. With a 250 μm spacer, at $t = 30$ min, a single peak appears associated with the void peak at t^0, which coincides with the location of unresolved species for all traces. This result is expected, since the spacer size was chosen to optimize separation of larger NPs at the later growth stages. The absence of a separated peak from the t^0 at $t = 30$ min in Fig. 3a suggests that the products are <10 nm, based on the fractionation conditions used for this measurement, and corroborated by TEM results (Fig. 1a).

The peak eluting at t^0 that contained gold seeds and initial growth products was evaluated using optimal fractionation conditions, which are provided in the ESM (Fig. S1). The evolution of peak shape and breadth are direct evidence of seed transformation, which can be further probed by altering fractionation conditions. Because isotropic growth of seed crystal occurs primarily at facets (100), (110), and (111), [15] further investigation of A4F capabilities to distinguish these populations using other similarly sized, metal faceted structures as calibrants is currently under investigation. Additionally, the concomitant growth of species observed after V_c removal provide direct evidence for transformation of seeds into larger structures. Although further work is

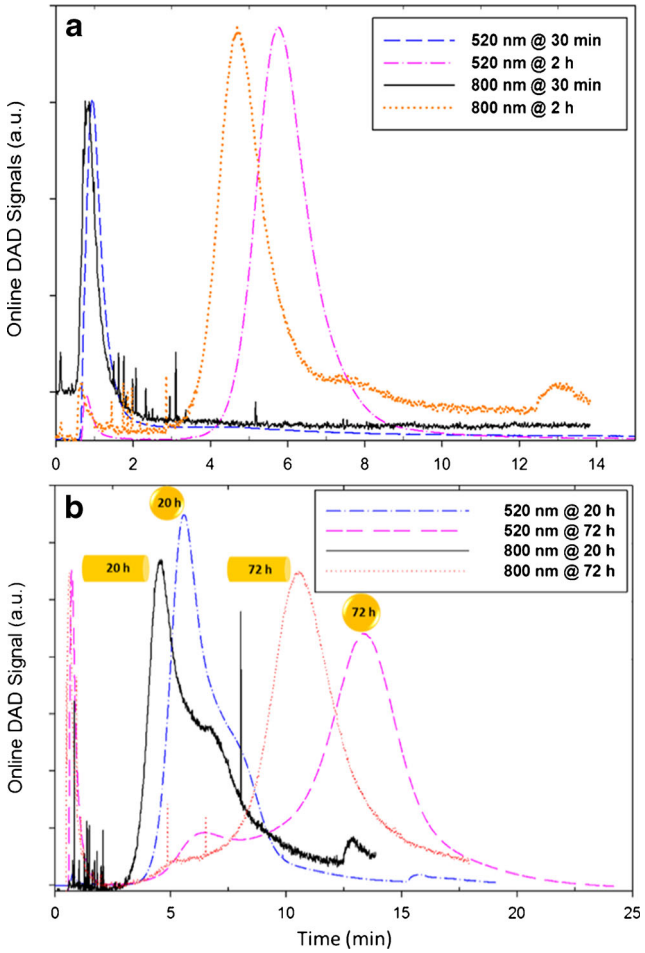

Fig. 3 Representative online DAD traces at 520 nm and 800 nm, characteristic optical signatures of NPs and NRs, respectively, during elution for GNRs analysed at defined sampling times during synthesis: **a** $0\ \text{h} < t \leq 2\ \text{h}$ and **b** $20\ \text{h} \leq t \leq 72\ \text{h}$. The traces at different wavelengths are extracted from the same runs. From $0\ \text{h} < t \leq 2\ \text{h}$, the conversion of sub-5 nm seeds to NPs and NRs is clearly observed by the appearance of peaks at $t_R > 3$ min for $t = 2$ h, and separation of NRs from NPs is clearly exhibited by the offset of characteristic traces for both shapes. The transition from small AR rods to longer rods and their distinct elution behaviour is depicted in panel b, where cartoon depictions indicate the shape and respective wavelengths used to follow their growth over time

necessary to characterize the burgeoning products in this size regime and to quantify distinct product populations, these results clearly demonstrate the capacity of the current method to probe the entire GNR synthesis product distribution.

At time $t = 2$ h, a peak was present with a retention time, t_R, of 6 min in the 520 nm trace (Fig. 3a). The appearance of a strong 520 nm peak clearly indicates the presence of AuNPs large enough to exhibit measurable SPR phenomena (roughly above 3 nm) [35]. The evolution of the peak follows the previous reported growth trends of GNRs in seed-mediated synthesis, where GNR formation occurs concurrently with the growth of the predominant product, spherical NPs, during initial formation (Fig. 1b) [15]. At the same reaction time ($t = 2$ h), an 800 nm elution peak is observed at $t_R = 5$ min, confirming the presence of GNRs with their characteristic red-shifted LSPR (Fig. 3a). In a recent study [31] focused on optimizing A4F to enhance separation of the principal high-AR GNR population from other product species (e.g., shorter rods, variably shaped particles), the high-AR rods were observed to elute after the "soup" containing NPs in the (50–60) nm size range. However, mechanisms for GNR elution over a wide parameter space of length, diameter, and AR have not been systematically studied due in part to the lack of available, uniform materials, which have led to the remainder of knowledge gaps on elution behavior for specific GNR populations.

The fractograms in Fig. 3b clearly illustrate the transition between the first and second phases of GNR growth. To more clearly depict the conversion from seeds to rods, we used the characteristic absorbances for each known species. At $t = 20$ h, a shoulder at $t_R \approx 7.5$ min was present in both 520 nm and 800 nm traces, suggesting that the development of GNRs continues well beyond growth initiation. The persistence of small (<10 nm) seeds remains evident at $t = 20$ h, as exhibited by the intensity at t^0, indicating that a subpopulation of seeds never evolve into GNRs or larger AuNPs; it has been established that GNR yields for seed-mediated synthesis can be as low as 4 % depending on the conditions (i.e., pH, temperature, reducing agent, etc.), [36] which were optimized iteratively to produce the GNR AR of interest. Evolution of GNRs can also be observed in the fractograms using a 254 nm trace (ESM Fig. S3), where nearly all species in the reaction mixture strongly absorb, thus providing a relative measure of mass change if, for convenience, absorbance is assumed to be uniform. Using this approach of assumed total mass in combination with reported intensities (i.e., molar extinction coefficients) of LSPR bands for different AR GNRs, quantitative evaluations of transformation yields from the seeds that result in GNR formation from populations lacking facets large enough to support micellar adsorption could begin to be developed. However, this would require high quality, uniform materials for calibration in these syntheses, which are highlighted by the observed coincidence of strong SPR related absorbance at t^0 for $t = 72$ h (Fig. 3b).

Although the trace at $t = 72$ h contains a distribution of products, distinction between the products can be achieved with the hyphenated A4F/UV-Vis system. Two distinct peaks are observed in the 520 nm trace, where the persistence of a peak at $t_R = 7.5$ min remains and the salient feature becomes the appearance of a peak near $t_R = 14$ min. It is hypothesized that this smaller 520 nm peak at $t_R = 7.5$ min corresponds to gold NPs (10 to 20) nm in diameter, based on the absence of GNR signatures in the online optical spectrum. These NPs presumably result from seeds that did not evolve into GNRs, but continued to grow in size. This is also supported by the high polydispersity of the solution as shown in Fig. 1c, where the broad 520 nm trace is observed. In addition, the maximum in the 800 nm trace shifts to longer times ($t = 11$ min) in

Fig. 3b, demonstrating continual growth of GNRs under these conditions for at least 72 h (i.e., no termination of GNR growth is observed). The coincidence of the local peak maxima at $t_R = 11$ min in the 520 nm and 800 nm traces is expected based on the known optical signature for the GNRs. In addition, the relatively high absorbance intensity at 800 nm in this region is consistent with the common observation that the LSPR bands are much stronger than the GNR-associated TSPR bands [13]. Overall, the results are consistent with an elution mechanism where spherical shaped nanomaterials elute more slowly than nanorods of comparable cross-section; however a more recent study [31] clearly shows larger spheres and low AR GNRs eluting before high AR (≈10) GNRs in a commercially sourced polydisperse product. It is fair to say that the mechanism of elution for GNRs over a wide parameter space of length, diameter, and shape remains unresolved, and is the focus of ongoing work.

To resolve some uncertainty about the elution mechanism and the polydispersity in shape in the present study, a commercially sourced CTAB coated GNR product with an established purity and AR was injected and fractionated under the same conditions as above. In Fig. S4 of the ESM, the fractograms are presented using 844 nm traces, which represent the observed absorbance maximum for the GNRs (AR = 4.52), for the seed-mediated products and the commercial material. A comparison of the commercial test material with our sample at $t = 72$ h exhibits good agreement for both traces. The elution profile of the commercial source is indicative of a monodisperse population that is likely a result of post synthesis separation and purification. However, our synthesized GNRs, which are known to have a similar diameter to the commercial source as confirmed by TEM, exhibit a similar t_R without extensive sample processing prior to examination, and further demonstrates the capacity of the current methods to probe the formation of GNRs from seeds to high AR (AR > 4) products. The consistency of the purified commercial and lab synthesized products provides a validated method to evaluate currently used synthesis parameters and other synthetic methods (e.g., ascorbic acid) online to probe specific transformations. This could in turn advance the development of improved procedures and higher GNR yields.

The advantages offered by tandem separation and characterization methods utilizing A4F are mainly achieved due to their non-disruptive nature, fast throughput, and in-situ analysis. To our knowledge, this is the first published in situ investigation of GNR growth, separation, and characterization using A4F. The utilization of A4F in this capacity is beyond traditional separation analysis. By using Hq as the reducing agent, the growth rate of GNRs could be monitored in real time using hyphenated A4F. Monitoring the LSPR absorbance reveals that GNRs in this case generally elute before their spherical counterparts. TEM confirmed that the number of peaks observed during fractionation corresponds with the size and shape dispersity expressed by retention behavior and optical signatures. The work presented here establishes a foundation for hyphenated A4F as a measurement technique that can be implemented in future mechanistic studies on the growth of GNRs from gold seeds, and thereby progress closer to the ultimate goal of rational design of these materials.

Acknowledgments Research performed in part at the NIST Center for Nanoscale Science and Technology, and funded in part by the NIST Nanomanufacturing Initiative through the Nanoparticle Manufacturing Program.

Compliance with ethical standards

Conflict of interest The authors declare no conflict of interest.

References

1. Zheng HM, Smith RK, Jun YW, Kisielowski C, Dahmen U, Alivisatos AP. Observation of single colloidal platinum nanocrystal growth trajectories. Science. 2009;324(5932):1309–12. doi:10.1126/science.1172104.
2. Senapati D, Singh AK, Khan SA, Senapati T, Ray PC. Probing real time gold nanostar formation process using two-photon scattering spectroscopy. Chem Phys Lett. 2011;504(1–3):46–51. doi:10.1016/j.cplett.2011.01.046.
3. Renaud G, Lazzari R, Revenant C, Barbier A, Noblet M, Ulrich O, et al. Real-time monitoring of growing nanoparticles. Science. 2003;300(5624):1416–9. doi:10.1126/science.1082146.
4. Grzelczak M, Sanchez-Iglesias A, Rodriguez-Gonzalez B, Alvarez-Puebla R, Perez-Juste J, Liz-Marzan LM. Influence of iodide ions on the growth of gold nanorods: tuning tip curvature and surface plasmon resonance. Adv Funct Mater. 2008;18(23):3780–6. doi:10.1002/adfm.200800706.
5. Bisker G, Yeheskely-Hayon D, Minai L, Yelin D. Controlled release of Rituximab from gold nanoparticles for phototherapy of malignant cells. J Control Release. 2012;162(2):303–9. doi:10.1016/j.jconrel.2012.06.030.
6. Murphy CJ, San TK, Gole AM, Orendorff CJ, Gao JX, Gou L, et al. Anisotropic metal nanoparticles: synthesis, assembly, and optical applications. J Phys Chem B. 2005;109(29):13857–70. doi:10.1021/jp0516846.
7. Park JH, von Maltzahn G, Xu MJ, Fogal V, Kotamraju VR, Ruoslahti E, et al. Cooperative nanomaterial system to sensitize, target, and treat tumors. Proc Natl Acad Sci U S A. 2010;107(3):981–6. doi:10.1073/pnas.0909565107.
8. Oyelere AK, Chen PC, Huang XH, El-Sayed IH, El-Sayed MA. Peptide-conjugated gold nanorods for nuclear targeting. Bioconjug Chem. 2007;18(5):1490–7. doi:10.1021/bc070132i.
9. Niidome T, Yamagata M, Okamoto Y, Akiyama Y, Takahashi H, Kawano T, et al. PEG-modified gold nanorods with a stealth character for in vivo applications. J Control Release. 2006;114(3):343–7. doi:10.1016/j.jconrel.2006.06.017.
10. Hauck TS, Jennings TL, Yatsenko T, Kumaradas JC, Chan WCW. Enhancing the toxicity of cancer chemotherapeutics with gold nanorod hyperthermia. Adv Mater. 2008;20(20):3832. doi:10.1002/adma.200800921.

11. Ma ZY, Xia HX, Liu YP, Liu B, Chen W, Zhao YD. Applications of gold nanorods in biomedical imaging and related fields. Chin Sci Bull. 2013;58(21):2530–6. doi:10.1007/s11434-013-5720-7.
12. Pissuwan D, Valenzuela SM, Cortie MB. Prospects for gold nanorod particles in diagnostic and therapeutic applications. Biotechnol Genet Eng Rev. 2008;25(25):93–112.
13. Lohse SE, Murphy CJ. The quest for shape control: a history of gold nanorod synthesis. Chem Mater. 2013;25(8):1250–61. doi:10.1021/cm303708p.
14. Polte J, Ahner TT, Delissen F, Sokolov S, Emmerling F, Thünemann AF, et al. Mechanism of gold nanoparticle formation in the classical citrate synthesis method derived from coupled in situ XANES and SAXS evaluation. J Am Chem Soc. 2010;132(4):1296–301. doi:10.1021/ja906506j.
15. Park K, Drummy LF, Wadams RC, Koerner H, Nepal D, Fabris L, et al. Growth mechanism of gold nanorods. Chem Mater. 2013;25(4):555–63. doi:10.1021/cm303659q.
16. Perez-Juste J, Liz-Marzan LM, Carnie S, Chan DYC, Mulvaney P. Electric-field-directed growth of gold nanorods in aqueous surfactant solutions. Adv Funct Mater. 2004;14(6):571–9. doi:10.1002/adfm.200305068.
17. Gole A, Murphy CJ. Seed-mediated synthesis of gold nanorods: role of the size and nature of the seed. Chem Mater. 2004;16(19):3633–40. doi:10.1021/cm0492336.
18. Mohamed MB, Ismail KZ, Link S, El-Sayed MA. Thermal reshaping of gold nanorods in micelles. J Phys Chem B. 1998;102(47):9370–4. doi:10.1021/jp9831482.
19. Link S, Burda C, Nikoobakht B, El-Sayed MA. Laser-induced shape changes of colloidal gold nanorods using femtosecond and nanosecond laser pulses. J Phys Chem B. 2000;104(26):6152–63. doi:10.1021/jp000679t.
20. Jana NR, Gearheart L, Obare SO, Murphy CJ. Anisotropic chemical reactivity of gold spheroids and nanorods. Langmuir. 2002;18(3):922–7. doi:10.1021/la0114530.
21. Tsung CK, Kou XS, Shi QH, Zhang JP, Yeung MH, Wang JF, et al. Selective shortening of single-crystalline gold nanorods by mild oxidation. J Am Chem Soc. 2006;128(16):5352–3. doi:10.1021/ja060447t.
22. Chandrasekar G, Mougin K, Haidara H, Vidal L, Gnecco E. Shape and size transformation of gold nanorods (GNRs) via oxidation process: a reverse growth mechanism. Appl Surf Sci. 2011;257(9):4175–9. doi:10.1016/j.apsusc.2010.12.015.
23. Vigderman L, Zubarev ER. High-yield synthesis of gold nanorods with longitudinal SPR peak greater than 1200 nm using hydroquinone as a reducing agent. Chem Mater. 2013;25(8):1450–7. doi:10.1021/cm303661d.
24. Edgar JA, McDonagh AM, Cortie MB. Formation of gold nanorods by a stochastic "Popcorn" mechanism. ACS Nano. 2012;6(2):1116–25. doi:10.1021/nn203586j.
25. Akbulut O, Mace CR, Martinez RV, Kumar AA, Nie ZH, Patton MR, et al. Separation of nanoparticles in aqueous multiphase systems through centrifugation. Nano Lett. 2012;12(8):4060–4. doi:10.1021/nl301452x.
26. Li SA, Chang Z, Liu JF, Bai L, Luo L, Sun XM. Separation of gold nanorods using density gradient ultracentrifugation. Nano Res. 2011;4(8):723–8. doi:10.1007/s12274-011-0128-7.
27. Gordel M, Olesiak-Banska J, Matczyszyn K, Nogues C, Pawlik K, Buckle M, Samoc M. Shape and size separation of gold nanoparticles using glucose gradient density. In: Andrews DL, Nunzi JM, Ostendorf A, editors. Nanophotonics Iv, vol 8424. Proceedings of SPIE. Proceedings of the SPIE, Brussels, Belgium; 2012. pp 1–7. doi:84242f.10.1117/12.922097.
28. Runyon JR, Goering A, Yong KT, Williams SKR. Preparation of narrow dispersity gold nanorods by asymmetrical flow field-flow fractionation and investigation of surface plasmon resonance. Anal Chem. 2013;85(2):940–8.
29. Gigault J, Cho TJ, MacCuspie RI, Hackley VA. Gold nanorod separation and characterization by asymmetric-flow field flow fractionation with UV-Vis detection. Anal Bioanal Chem. 2013;405(4):1191–202. doi:10.1007/s00216-012-6547-9.
30. Nguyen TM, Gigault J, Hackley VA. PEGylated gold nanorod separation based on aspect ratio: characterization by asymmetric-flow field flow fractionation with UV-Vis detection. Anal Bioanal Chem. 2014;406(6):1651–9. doi:10.1007/s00216-013-7318-y.
31. Nguyen T, Liu J, Hackley V. Fractionation and characterization of high aspect ratio gold nanorods using asymmetric-flow field flow fractionation and single particle inductively coupled plasma mass spectrometry. Chromatography. 2015;2(3):422.
32. Gigault J, Pettibone JM, Schmitt C, Hackley VA. Rational strategy for characterization of nanoscale particles by asymmetric-flow field flow fractionation: a tutorial. Anal Chim Acta. 2014;809:9–24. doi:10.1016/j.aca.2013.11.021.
33. Lin WH, Lu YH, Hsu YJ. Au nanoplates as robust, recyclable SERS substrates for ultrasensitive chemical sensing. J Colloid Interface Sci. 2014;418:87–94. doi:10.1016/j.jcis.2013.11.082.
34. Chu HC, Kuo CH, Huang MH. Thermal aqueous solution approach for the synthesis of triangular and hexagonal gold nanoplates with three different size ranges. Inorg Chem. 2006;45(2):808–13. doi:10.1021/ic051758s.
35. El-Brolossy TA, Abdallah T, Mohamed MB, Abdallah S, Easawi K, Negm S, et al. Shape and size dependence of the surface plasmon resonance of gold nanoparticles studied by photoacoustic technique. Eur Phys J Spec Top. 2008;153(1):361–4. doi:10.1140/epjst/e2008-00462-0.
36. Jana NR, Gearheart L, Murphy CJ. Wet chemical synthesis of high aspect ratio cylindrical gold nanorods. J Phys Chem B. 2001;105(19):4065–7. doi:10.1021/jp0107964.